CHEMISTRY
A EUROPEAN JOURNAL

DOI: 10.1002/chem.200902047

One-Dimensional Ferromagnetically Coupled Bimetallic Chains Constructed with *trans*-$[Ru(acac)_2(CN)_2]^-$: Syntheses, Structures, Magnetic Properties, and Density Functional Theoretical Study

Jun-Fang Guo,[a] Xiu-Teng Wang,[b] Bing-Wu Wang,[b] Guan-Cheng Xu,[b] Song Gao,*[b] Lap Szeto,[c] Wing-Tak Wong,[c] Wai-Yeung Wong,[d] and Tai-Chu Lau*[a]

Abstract: Four cyano-bridged 1D bimetallic polymers have been prepared by using the paramagnetic building block *trans*-$[Ru(acac)_2(CN)_2]^-$ (Hacac = acetylacetone): $\{[\{Ni(tren)\}\{Ru(acac)_2(CN)_2\}][ClO_4]\cdot CH_3OH\}_n$ (**1**) (tren = tris(2-aminoethyl)amine), $\{[\{Ni(cyclen)\}\{Ru(acac)_2(CN)_2\}][ClO_4]\cdot CH_3OH\}_n$ (**2**) (cyclen = 1,4,7,10-tetraazacyclododecane), $\{[\{Fe(salen)\}\{Ru(acac)_2(CN)_2\}]\}_n$ (**3**) ($salen^{2-}$ = *N*,*N*′-bis(salicylidene)-*o*-ethyldiamine dianion) and $[\{Mn(5,5'\text{-}Me_2salen)\}_2\{Ru(acac)_2(CN)_2\}][Ru(acac)_2(CN)_2]\cdot 2CH_3OH$ (**4**) (5,5′-Me_2salen = *N*,*N*′-bis(5,5′-dimethylsalicylidene)-*o*-ethylenediimine). Compounds **1** and **2** are 1D, zigzagged NiRu chains that exhibit ferromagnetic coupling between Ni^{II} and Ru^{III} ions through cyano bridges with $J = +1.92\ cm^{-1}$, $zJ' = -1.37\ cm^{-1}$, $g = 2.20$ for **1** and $J = +0.85\ cm^{-1}$, $zJ' = -0.16\ cm^{-1}$, $g = 2.24$ for **2**. Compound **3** has a 1D linear chain structure that exhibits intrachain ferromagnetic coupling ($J = +0.62\ cm^{-1}$, $zJ' = -0.09\ cm^{-1}$, $g = 2.08$), but antiferromagnetic coupling occurs between FeRu chains, leading to metamagnetic behavior with $T_N = 2.6$ K. In compound **4**, two Mn^{III} ions are coordinated to *trans*-$[Ru(acac)_2(CN)_2]^-$ to form trinuclear Mn_2Ru units, which are linked together by π–π stacking and weak Mn···O* interactions to form a 1D chain. Compound **4** shows slow magnetic relaxation below 3.0 K with $\phi = 0.25$, characteristic of superparamagnetic behavior. The $Mn^{III}\cdots Ru^{III}$ coupling constant (through cyano bridges) and the $Mn^{III}\cdots Mn^{III}$ coupling constant (between the trimers) are +0.87 and $+0.24\ cm^{-1}$, respectively. Compound **4** is a novel single-chain magnet built from Mn_2Ru trimers through noncovalent interactions. Density functional theory (DFT) combined with the broken symmetry state method was used to calculate the molecular magnetic orbitals and the magnetic exchange interactions between Ru^{III} and M (M = Ni^{II}, Fe^{III}, and Mn^{III}) ions. To explain the somewhat unexpected ferromagnetic coupling between low-spin Ru^{III} and high-spin Fe^{III} and Mn^{III} ions in compounds **3** and **4**, respectively, it is proposed that apart from the relative symmetries, the relative energies of the magnetic orbitals may also be important in determining the overall magnetic coupling in these bimetallic assemblies.

Keywords: coordination modes · density functional calculations · magnetic properties · molecule-based magnets · ruthenium · single-chain magnets

[a] Dr. J.-F. Guo, Prof. T.-C. Lau
Department of Biology and Chemistry
City University of Hong Kong, Tat Chee Avenue
Kowloon Tong, Hong Kong (China)
Fax: (+852) 27887406
E-mail: bhtclau@cityu.edu.hk

[b] Dr. X.-T. Wang, Dr. B.-W. Wang, Dr. G.-C. Xu, Prof. S. Gao
Beijing National Laboratory for Molecular Sciences
State Key Laboratory of Rare Earth Materials
Chemistry and Applications
College of Chemistry and Molecular Engineering
Peking University, Beijing 100871 (China)
Fax: (+86) 1062751708
E-mail: gaosong@pku.edu.cn

[c] L. Szeto, Prof. W.-T. Wong
Department of Chemistry, The University of Hong Kong
Pokfulam Road, Hong Kong (China)

[d] Prof. W.-Y. Wong
Department of Chemistry, Hong Kong Baptist University
Waterloo Road, Kowloon, Hong Kong (China)

Supporting information for this article is available on the WWW under http://dx.doi.org/10.1002/chem.200902047.

Introduction

Paramagnetic 3d cyanometalates, $[M(CN)_6]^{n-}$ and $[M(L)_y(CN)_x]^{q-}$ (L = ancilliary ligand), have long been used as building blocks for the construction of a wide variety of molecule-based materials; many of them exhibit novel magnetic properties.[1–4] The nature of the magnetic interaction between 3d metal centers in these compounds is usually governed by the relative symmetries of the magnetic orbitals.[1,2] In recent years, the preparation of molecule-based materials has been extended to 4d and 5d metal ions, since their orbitals are more diffuse and so enhanced magnetic interactions may be expected. We were interested in preparing polynuclear complexes based on paramagnetic ruthenium(III) building blocks.[5] Although $[Fe(CN)_6]^{3-}$ is robust and readily available, $[Ru(CN)_6]^{3-}$ is very unstable, especially in solvents such as water and alcohols.[6] On the other hand, $[Ru(ox)_3]^{3-}$ is much more stable and a number of coordination polymers of the general formula $[NBu_4][M^{II}Ru^{III}(ox)_3]$ (M = Mn, Fe and Cu) have been reported.[7] The drawback of using $[Ru(ox)_3]^{3-}$ as a building block, at least in our hands, is that the coordination polymers produced are mostly in powder form and single crystals suitable for X-ray crystal structure determination are difficult to obtain. Recently, we and others reported the use of two dicyanoruthenate(III) complexes, *trans*-$[Ru^{III}(acac)_2(CN)_2]^-$ (Hacac = acetylacetone) and *trans*-$[Ru^{III}(salen)(CN)_2]^-$ (salen = *N*,*N*-bis(salicylidene)ethylenediamine), as building blocks. A number of trimeric, 1D, 2D, and 3D bimetallic compounds can be readily obtained by treatment of these building blocks with 3d metal centers (M^N). These compounds have been structurally characterized by X-ray crystallography, and they exhibit various magnetic behaviors (Table 1).[5,7] However, the nature of M^N–Ru^{III} interactions in some of these compounds cannot be readily rationalized using Kahn's orbital symmetry model. For example, although in the trinuclear $[Mn^{II}(CH_3OH)_4\{Ru(salen)(CN)_2\}_2]$ and 2D $\{[Mn^{II}(H_2O)_2\{Ru(salen)(CN)_2\}_2]\cdot H_2O\}_n$ the Mn^{II}–Ru^{III} interaction is antiferromagnetic,[5b] which is as expected; in the 1D $[\{Mn^{III}(L)\}\{Ru(salen)(CN)_2\}]$ (L is a salen type ligand)[5f] the Mn^{III}–Ru^{III} interaction is ferromagnetic. Thus, it is worthwhile to study more M^N–Ru^{III} systems in order to gain a better understanding of the nature of M^N–Ru^{III} magnetic interactions.

Herein, we report the syntheses, structures, and magnetic properties of four new bimetallic compounds constructed from $[Ru(acac)_2(CN)_2]^-$; $\{[\{Ni(tren)\}\{Ru(acac)_2(CN)_2\}][ClO_4]\cdot CH_3OH\}_n$ (tren = tris(2-aminoethyl)amine) (**1**), $\{[\{Ni(cyclen)\}\{Ru(acac)_2(CN)_2\}][ClO_4]\cdot CH_3OH\}_n$ (cyclen = 1,4,7,10-tetraazacyclododecane) (**2**), $\{[\{Fe(salen)\}\{Ru(acac)_2(CN)_2\}]\}_n$ (**3**), $[\{Mn(5,5'\text{-}Me_2salen)\}_2\{Ru(acac)_2(CN)_2\}][Ru(acac)_2(CN)_2]\cdot 2CH_3OH$ (5,5′-Me_2salen = *N*,*N*′-bis(5,5′-dimethylsalicylidene)-*o*-ethylenediimine) (**4**). Compounds **1** and **2** have a 1D zigzagged chain structure, which is different from the linear chain structure of $[\{Ni^{II}(cyclam)\}\{Ru^{III}(salen)(CN)_2\}][ClO_4]$.[5e] Compound **3** is the first example of an $Fe^{III}Ru^{III}$ coordination polymer. It exhibits metamagnetic behavior with $T_N = 2.6$ K. Compound **4** is a novel single-chain magnet built from Mn_2Ru trimers linked together by noncovalent interactions. DFT calculations have also been performed on compounds **1**, **3**, and **4**, which provide insight into the nature of magnetic interactions in M^N-Ru^{III} bimetallic assemblies.

Results and Discussion

Synthesis and characterization: Reaction of *trans*-$Ph_4P[Ru(acac)_2(CN)_2]$ (Ph = phenyl) with the partially blocked complexes $[Ni(tren)][ClO_4]_2$, $[Ni(cyclen)][ClO_4]_2$, $[Fe(salen)(OAc)]$ (OAc = acetate) and $[Mn(5,5'\text{-}Me_2salen)]PF_6$ in methanol/DMF or methanol resulted in the formation of respective complexes **1**–**4**. The IR spectra show ν_{CN} stretches at 2137(s) for **1**, 2133(s) for **2**, 2118(s) for **3**, and 2120(s) and 2090 cm^{-1}(m) for **4**. The two peaks for **4** are assigned to the bridging and terminal cyanide stretches, respectively. In each compound, a cyanide stretch occurring at a higher frequency than that of the monomeric complex *trans*-$Ph_4P[Ru(acac)_2(CN)_2]$ (2096 cm^{-1}) is observed, indicating coordination of cyanide to a second metal.

Table 1. Summary of M^NRu^{III} bimetallic compounds.

Compounds	Structure	Ru^{III}-M interaction/magnetic properties	Ref.
$[Bu_4N][Cu^{II}Ru^{III}(ox)_3]$	2D	AF	[7]
$[Bu_4N][Fe^{II}Ru^{III}(ox)_3]$	2D	AF ferromagnet, $T_N = 13$ K	
$[Bu_4N][Mn^{II}Ru^{III}(ox)_3]$	2D	F	
$\{[M\{Ru(acac)_2(CN)_2\}_2]\}_n$[a]	3D diamond-like	F ferromagnet, $T_C = 3.6$ K (Mn), 4.6 K (Co)	[5a,b]
$[Ni(cyclam)\{Ru(acac)_2(CN)_2\}_2]\cdot 2CH_3OH\cdot 2H_2O$	trinuclear	F	[5b]
$Ph_4P[Ln(NO_3)_2\{Ru(acac)_2(CN)_2\}_2]$[b]	2D	negligible	[5c]
$[\{Ru(acac)_2(CN)_2\}\{Ni_2(L)(H_2O)_2\}][Ru(acac)_2(CN)_2]\cdot 2H_2O$[c]	1D	F Ni–Ni: AF, overall AF	[5d]
$[\{Ru(acac)_2(CN)_2\}\{Co(dmphen)(NO_3)\}]\cdot H_2O$	1D	F	
$[\{Ru(acac)_2(CN)_2\}\{Ni(dmphen)(NO_3)\}]\cdot H_2O$	1D	F	
$[Mn^{II}(CH_3OH)_4\{Ru(salen)(CN)_2\}_2]\cdot 6CH_3OH\cdot 2H_2O$	trinuclear	AF	[5b]
$\{[\{Mn^{II}(H_2O)_2\}\{Ru(salen)(CN)_2\}_2]\cdot H_2O\}_n$	2D	AF	
$[\{Ni^{II}(cyclam)\}\{Ru^{III}(salen)(CN)_2\}][ClO_4]$	1D	F	[5e]
$[\{Mn^{III}(L)\}\{Ru(salen)(CN)_2\}]$[d]	1D	F metamagnet, $T_N = 2.5$ K	[5f]

[a] M = Mn, Co. [b] Ln = Tb, Dy, Er, Gd. [c] L = a binucleating Schiff-base ligand. [d] L = a salen type ligand.

Table 2. Summary of crystallographic data for compounds **1–4**.

	1	**2**	**3**	**4**
formula	$C_{19}H_{36}ClN_6NiO_9Ru$	$C_{21}H_{38}N_6NiO_9RuCl$	$C_{28}H_{28}FeN_4O_6Ru$	$C_{62}H_{72}Mn_2N_8O_{14}Ru_2$
μ_r	687.77	713.80	673.46	1465.30
crystal system	triclinic	monoclinic	triclinic	monoclinic
space group	$P\bar{1}$	$P2_1/c$	$P\bar{1}$	$P2_1/c$
a [Å]	7.9467(19)	12.3160 (8)	71.3124(4)	13.9757(8)
b [Å]	13.345(3)	14.9247 (9)	12.3476(7)	15.0538(8)
c [Å]	13.807(3)	16.7362 (11)	15.8104(9)	16.5309(9)
α [°]	93.572(3)	90	89.98(0)	90.00
β [°]	104.321(3)	100.074 (1)	78.75(0)	111.67(0)
γ [°]	93.847(3)	90	79.66(0)	90.00
V [Å^3]	1410.8(6)	3028.9 (3)	1376.46(13)	3232.05(30)
Z	2	4	2	2
ρ_{calcd} [g cm^{-3}]	1.619	1.565	1.625	1.506
T [K]	301 (2)	296 (2)	173(2)	301 (2)
μ [mm^{-1}]	1.352	1.26	1.125	0.909
F(000)	706.0	1468	684	1500
data/restraints/parameters	6244/25/338	6890/0/335	6329/0/354	7370/1/401
GOF on F^2	1.061	1.045	1.024	1.018
R_1, wR_2 [$I>2\sigma(I)$]	0.154, 0.055	0.122, 0.043	0.078, 0.033	0.083, 0.031
R_1, wR_2(all data)	0.069, 0.164	0.061, 0.135	0.052, 0.087	0.046, 0.094

X-ray crystal structures: Crystallographic data for compounds **1–4** are listed in Table 2, and selected bond lengths and angles in Tables 3–6, respectively.

*Compound **1***: Single-crystal X-ray analysis reveals that **1** has a 1D, zigzagged chain-structure with each $[Ru(acac)_2(CN)_2]^-$ unit connected to two $[Ni(tren)]^{2+}$ units through the *trans* cyano groups, forming an almost planar -Ru-CN-Ni-NC- polymeric backbone. The perchlorate anions and methanol solvates are situated between the polymeric chains (Figure 1, bottom and Figure S1 in the Supporting Information). Each Ni^{II} center is octahedrally coordinated to the four nitrogen atoms of tren and two nitrogen atoms of the cyano groups in a *cis* configuration. The Ni–N(tren) (2.106(4)–2.140(4) Å) and the Ni–N(cyanido) bond lengths (2.041(4), 2.106(4) Å) in compound **1** (Table 3) are compara-

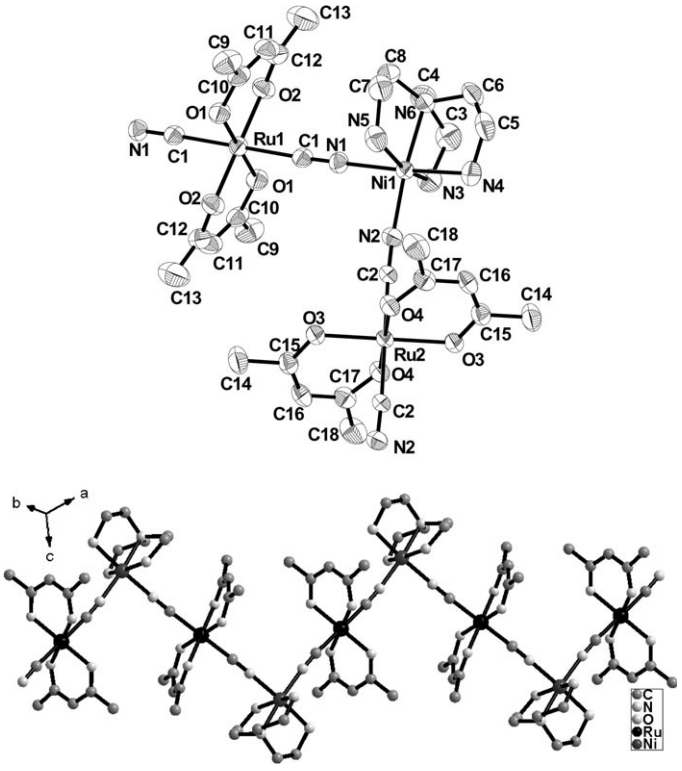

Figure 1. Top: ORTEP view of **1** with the atom labeling scheme. Bottom: view of the 1D zigzag chain of **1**. Hydrogen atoms, anion ClO_4^- and solvated methanol molecules are omitted for clarity.

Table 3. Selected bond lengths [Å] and angles [°] for compound **1**.[a]

Ru1–O1	2.011 (3)	Ni1–N2	2.041 (4)
Ru1–O2	2.011 (4)	Ni1–N6	2.106 (4)
Ru1–C1	2.059 (5)	Ni1–N1	2.106 (4)
Ru2–O3	2.007 (3)	Ni1–N4	2.108 (4)
Ru2–O4	2.022 (3)	Ni1–N3	2.135 (4)
Ru2–C2	2.064 (5)	Ni1–N5	2.140 (4)
N1–C1	1.149 (7)	N2–C2	1.156 (6)
$O2^i$-Ru1-O2	180.000 (1)	O3-Ru2-$O3^{ii}$	180.000 (1)
$O1^i$-Ru1-O1	180.00 (19)	O4-Ru2-$O4^{ii}$	180.00 (16)
O2-Ru1-$O1^i$	89.36 (15)	$O3^{ii}$-Ru2-O4	89.73 (13)
O2-Ru1-O1	90.64 (15)	O3-Ru2-O4	90.27 (13)
$O2^i$-Ru1-C1	88.10 (18)	O3-Ru2-$C2^{ii}$	91.03 (16)
O2-Ru1-C1	91.90 (18)	O4-Ru2-$C2^{ii}$	94.66 (16)
$O1^i$-Ru1-C1	88.93 (16)	O3-Ru2-C2	88.97 (16)
O1-Ru1-C1	91.07 (16)	O4-Ru2-C2	85.34 (16)
C1-Ru1-$C1^i$	180.000 (1)	$C2^{ii}$-Ru2-C2	180.0 (2)
N2-Ni1-N6	174.22 (17)	N2-Ni1-N3	97.31 (18)
N2-Ni1-N1	91.64 (17)	N6-Ni1-N3	82.14 (18)
N6-Ni1-N1	94.07 (17)	N1-Ni1-N3	86.57 (18)
N2-Ni1-N4	91.72 (19)	N4-Ni1-N3	94.59 (19)
N6-Ni1-N4	82.61 (19)	N2-Ni1-N5	99.83 (19)
N1-Ni1-N4	176.28 (18)	N6-Ni1-N5	81.51 (18)
N3-Ni1-N5	161.5 (2)	N1-Ni1-N5	85.96 (18)
N4-Ni1-N5	91.9 (2)	C1-N1-Ni1	178.8 (4)
N1-C1-Ru1	177.8 (5)	C2-N2-Ni1	173.6 (4)
N2-C2-Ru2	172.6 (4)		

[a] Symmetry codes: i: $-x$, $2-y$, $1-z$; ii: $1-x$, $1-y$, $1-z$.

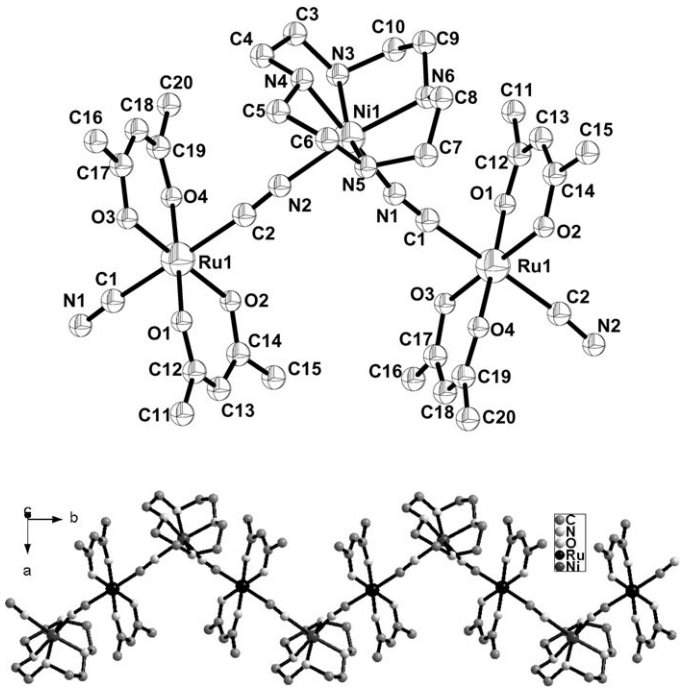

Figure 2. Top: ORTEP view of **2** with the atom labeling scheme. Bottom: view of the 1D zigzag chain of **2**. Hydrogen atoms, anion ClO_4^- and solvated methanol molecules are omitted for clarity.

ble to those in $[(\{Ni(tren)\}_3\{Fe(CN)_6\})_2]\cdot 6H_2O$.[8] The Ni–N≡C units are virtually linear with angles of 178.8(4) and 173.6(4)°; whereas the N2-Ni-N1 unit is bent with angle of 91.64(17)°, leading to a zigzagged chain. The bond lengths in each $[Ru(acac)_2(CN)_2]^-$ unit [Ru–O = 2.007(3)–2.022(3) Å; Ru–C = 2.059(5)–2.064(5) Å, C≡N = 1.149(7)–1.156(6) Å] are similar to those of the monomeric complex *trans*-$Ph_4P[Ru(acac)_2(CN)_2]$[5a] (Ru–O = 1.98(2)–2.03(2) Å; Ru–C = 2.06(3)–2.09(3) Å; C≡N = 1.12(3)–1.15(3) Å) and other bimetallic compounds containing $[Ru(acac)_2$-

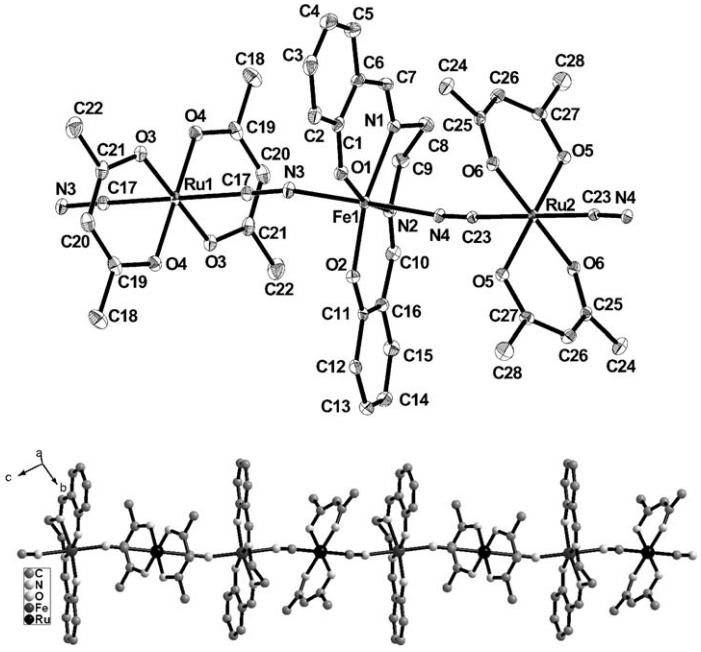

Figure 3. Top: ORTEP view of **3** with the atom labeling scheme. Bottom: view of the linear chain of **3**.

Table 4. Selected bond lengths [Å] and angles [°] for compound **2**.[a]

Ru1–O3	2.000 (3)	Ni1–N2	2.057 (3)
Ru1–O4	2.009 (3)	Ni1–N1	2.080 (3)
Ru1–O2	2.011 (3)	Ni1–N6	2.094 (4)
Ru1–O1	2.014 (3)	Ni1–N4	2.096 (3)
Ru1–C1	2.059 (4)	Ni1–N5	2.125 (4)
Ru1–C2	2.064 (4)	Ni1–N3	2.133 (4)
N1–C1	1.141 (5)	N2–C2^{i}	1.146 (5)
O3-Ru1-O4	90.77 (12)	N2-Ni1-N1	87.48 (14)
O3-Ru1-O2	177.60 (12)	N2-Ni1-N6	172.08 (14)
O4-Ru1-O2	90.97 (12)	N1-Ni1-N6	84.82 (14)
O3-Ru1-O1	88.12 (12)	N2-Ni1-N4	91.67 (14)
O4-Ru1-O1	178.34 (12)	N1-Ni1-N4	178.27 (15)
O2-Ru1-O1	90.17 (11)	N6-Ni1-N4	96.07 (14)
O3-Ru1-C1	93.86 (14)	N2-Ni1-N5	96.75 (14)
O4-Ru1-C1	90.48 (14)	N1-Ni1-N5	101.16 (15)
O2-Ru1-C1	87.78 (14)	N6-Ni1-N5	82.93 (15)
O1-Ru1-C1	88.36 (13)	N4-Ni1-N5	80.44 (14)
O3-Ru1-C2	88.08 (13)	N2-Ni1-N3	99.94 (15)
O4-Ru1-C2	86.12 (14)	N1-Ni1-N3	97.83 (15)
O2-Ru1-C2	90.38 (14)	N6-Ni1-N3	83.01 (15)
O1-Ru1-C2	95.07 (14)	N4-Ni1-N3	80.83 (14)
C1-Ru1-C2	176.11 (15)	N5-Ni1-N3	155.17 (14)
N1-C1-Ru1	173.3 (4)	C1-N1-Ni1	167.8 (3)
N2^{ii}-C2-Ru1	172.7 (4)	C2^{i}-N2-Ni1	171.1 (3)

[a] Symmetry codes: i: $-x$, $y-1/2$, $-z+1/2$; ii: $-x$, $y+1/2$, $-z+1/2$.

Table 5. Selected bond lengths [Å] and angles [°] for compound **3**.[a]

Fe1–O1	1.910(3)	O3–Ru1	2.008(2)
Fe1–O2	1.912(2)	O4–Ru1	2.010(2)
Fe1–N3	2.121(3)	O5–Ru2	2.004(2)
Fe1–N4	2.133(3)	O6–Ru2	2.016(2)
Fe1–N2	2.135(3)	C17–Ru1	2.062(3)
Fe1–N1	2.144(3)	C23–Ru2	2.065(3)
C17–N3	1.151(4)	C23–N4	1.148(4)
O1-Fe1-O2	109.31(9)	O3-Ru1-O3^{i}	180.00(9)
O1-Fe1-N3	89.32(10)	O3-Ru1-O4^{i}	90.30(9)
O2-Fe1-N3	90.63(9)	O3-Ru1-O4	89.70(9)
O1-Fe1-N4	88.77(9)	O4^{i}-Ru1-O4	179.99(9)
O2-Fe1-N4	88.72(9)	O3-Ru1-C17^{i}	92.72(10)
N3-Fe1-N4	177.66(10)	O3-Ru1-C17	87.28(10)
O1-Fe1-N2	162.15(9)	O4-Ru1-C17	93.14(10)
O2-Fe1-N2	87.89(9)	O4-Ru1-C17^{i}	86.86(10)
N3-Fe1-N2	85.65(10)	C17^{i}-Ru1-C17	180.00(11)
N4-Fe1-N2	96.57(10)	O5-Ru2-O5^{ii}	180.00(8)
O1-Fe1-N1	87.63(10)	O5-Ru2-O6	89.90(8)
O2-Fe1-N1	162.17(9)	O5-Ru2-O6^{ii}	90.10(8)
N3-Fe1-N1	95.23(10)	O6-Ru2-O6^{ii}	179.98(8)
N4-Fe1-N1	86.05(10)	O5-Ru2-C23	87.3(1)
N2-Fe1-N1	75.82(10)	O5^{ii}-Ru2-C23	92.7(1)
C17-N3-Fe1	166.98(23)	O6-Ru2-C23	89.25(9)
C23-N4-Fe1	160.99(23)	O6^{ii}-Ru2-C23	90.75(9)
N3-C17-Ru1	175.68(24)	C23-Ru2-C23^{ii}	179.99(11)
N4-C23-Ru2	176.62(24)		

[a] Symmetry codes: i: $-x$, $-y$, $1-z$; ii: $1-x$, $1-y$, $-z$.

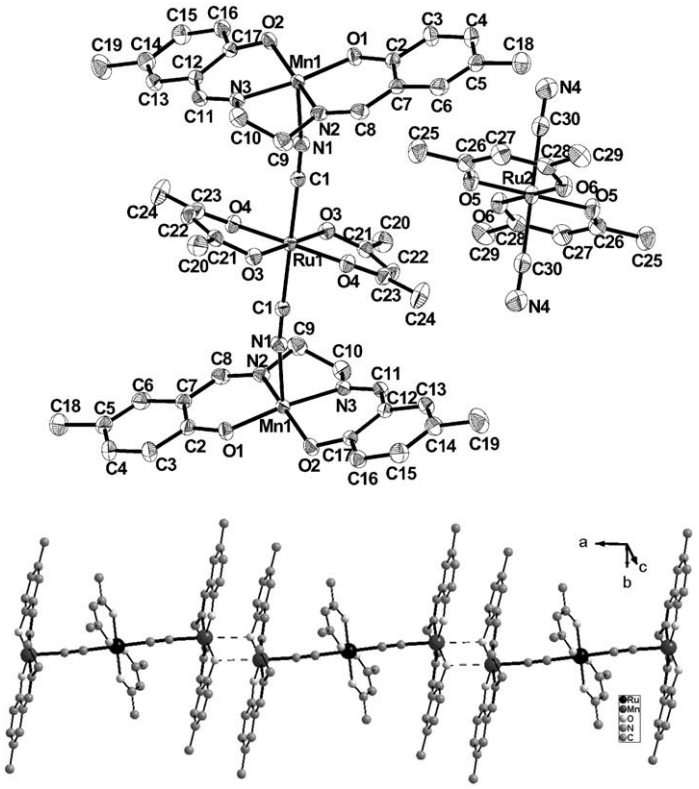

Figure 4. Top: ORTEP plot of **4** (30% probability ellipsoids). The methanol solvates were omitted for clarity. Middle: 1D assembly of Mn^{III}–Ru^{III}–Mn^{III} trinuclear units in **4**. Bottom: crystal packing diagram of **4** with hydrogen atoms omitted for clarity.

$(CN)_2]^-$.[5a–d] The Ru–C≡N angles (172.6(4)–177.8(5)°) are close to linear (Figure 1, top). The closest intramolecular Ni···Ru distance is 5.232 Å and the closest intermolecular Ru···Ru separation is 7.533 Å.

Table 6. Selected bond lengths [Å] and angles [°] for compound **4**.[a]

Ru1–O3	2.0086 (17)	Mn1–O1	1.8538 (17)
Ru1–O4	2.0171 (16)	Mn1–O2	1.8776 (18)
Ru1–C1	2.060 (2)	Mn1–N3	1.971 (2)
Ru2–O6	2.0094 (18)	Mn1–N2	1.976 (2)
Ru2–O5	2.0103 (18)	Mn1–N1	2.165 (2)
Ru2–C30	2.067 (3)	N4–C30	1.143 (4)
N1–C1	1.144 (3)		
O3-Ru1-O4^{i}	89.90 (7)	O5^{ii}-Ru2-C30	89.53 (10)
O3-Ru1-O4	90.10 (7)	O6-Ru2-O5	91.45 (8)
O3-Ru1-O3^{i}	180.0	O6-Ru2-O6^{ii}	180.0
O4^{i}-Ru1-O4	180.00 (6)	C30-Ru2-C30^{ii}	180.00 (13)
C1^{i}-Ru1-C1	180.0	O5-Ru2-O5^{ii}	180.0
O3-Ru1-C1^{i}	90.38 (8)	O6^{ii}-Ru2-O5	88.55 (8)
O4-Ru1-C1^{i}	93.68 (8)	O6-Ru2-C30	90.48 (10)
O3-Ru1-C1	89.62 (8)	O6^{ii}-Ru2-C30	89.52 (10)
O4-Ru1-C1	86.32 (8)	O5-Ru2-C30	90.47 (10)
O1-Mn1-O2	92.20 (8)	N3-Mn1-N2	82.90 (9)
O1-Mn1-N3	168.02 (8)	O1-Mn1-N1	101.18 (8)
O2-Mn1-N3	89.85 (8)	O2-Mn1-N1	102.53 (9)
O1-Mn1-N2	92.13 (8)	N3-Mn1-N1	89.87 (8)
O2-Mn1-N2	164.27 (9)	N2-Mn1-N1	91.44 (9)
N1-C1-Ru1	177.3 (2)	C1-N1-Mn1	168.1 (2)
N4-C30-Ru2	178.3 (3)		

[a] Symmetry codes: i: $-x+1, -y+1, -z+1$; ii: $-x+1, -y, -z+1$.

Compound ***2***: The structure of **2** is similar to that of **1**, it also has a 1D, zigzagged chain-structure formed by assembly of the $[Ru(acac)_2(CN)_2]^-$ and $[Ni(cyclen)]^{2+}$ ions through bridging cyano groups. The perchlorate anions and methanol solvates are situated between the polymeric chains (Figure 2, bottom). Each Ni^{II} center is octahedrally coordinated to the four nitrogen atoms of cyclen and two nitrogen atoms of cyano groups in a *cis* configuration. The Ni–N(cyclen) (2.094(4)–2.133(4) Å) and the Ni–N(cyanido) bond lengths (2.057(3), 2.080(3) Å) in compound **2** (Table 4) are comparable to those in $\{[\{Ni(cyclen)\}\{Mn(N)(CN)_4\}]\cdot CH_3OH\}_n$[9] and $[Ni(cyclen)]_2[Pt(CN)_4]_2\cdot 6H_2O$.[10] The Ni–N≡C units are bent with angles of 167.8(3) and 171.1(3)°; the N2-Ni-N1 unit is also bent with an angle of 87.48(14)°, resulting in a zigzagged chain. The bond lengths in each $[Ru(acac)_2(CN)_2]^-$ unit (Ru–O = 2.000(3)–2.014(3) Å; Ru–C = 2.059(4)–2.064(4) Å; C≡N = 1.141(5)–1.146(5) Å) are similar to those found in compound **1**. The Ru–C≡N angles (172.7(4)–173.3(4)°) are close to linear (Figure 2, top). The closest intramolecular Ni···Ru distance is 5.225 (5) Å and the closest intermolecular Ru···Ru and Ni···Ni separations are 7.574(4) Å and 8.4493(7) Å, respectively.

Compound ***3***: Compound **3** has a 1D linear chain structure with each $[Ru(acac)_2(CN)_2]^-$ unit connected to two $[Fe(salen)]^+$ units through the *trans* cyano groups (Figure 3 and Figure S2 in the Supporting Information). The mean Ru–O(acac) (2.007(2) Å) and Ru–C (2.064(3) Å) bond lengths (Table 5) are similar to those in other Ru^{III}–M bimetallic

complexes.[5a–d] The Ru–C≡N angles are close to linear (175.68(24)° for Ru1-C17-N3 and 176.62(24)° for Ru2-C23-N4). Each Fe^{III} center is octahedrally coordinated to the two nitrogen atoms and two oxygen atoms of salen and two nitrogen atoms of cyano groups in a *trans* configuration. The Fe–N(salen) (2.135(3)–2.144(3) Å), Fe–O(salen) (1.910(3)–1.912(2) Å) and Fe–N(cyanido) bond lengths (2.121(3), 2.133(3) Å) in compound **3** are comparable to those in $[\{Fe(salen)\}_3\{Fe(CN)_6\}(MeOH)_2]_n \cdot 3n H_2O$.[11] The Fe–N≡C units are bent with angles of 166.98(23) and 160.99(23)°. The closest intramolecular Fe···Ru distance is 5.300 Å and the closest intermolecular Ru···Ru and Fe···Fe separations are both 7.312 Å.

*Compound **4***: As depicted in Figure 4 (top), the basic unit of **4** is composed of two $[Mn(5,5'\text{-}Me_2salen)]^+$ ions joined with one $[Ru(acac)_2(CN)_2]^-$ ion to form a cyano-bridged linear trinuclear cation $[Mn\text{-}NC\text{-}Ru\text{-}CN\text{-}Mn]^+$. The $[Mn(5,5'\text{-}Me_2salen)]^+$ units are further linked together by intermolecular face-to-face π–π interactions between neighboring (5,5′-Me_2salen) ligands (with an average separation of about 3.38 Å) and weak Mn···O*(phenolate oxygen of the adjacent $[Mn^{III}(5,5'\text{-}Me_2salen)]^+$ unit) interactions, resulting in a 1D, linear chain structure (Figure 4, middle). The Mn···O* distance of 2.921 Å is much longer than that of a dimeric Mn^{III}–salen analogue (2.375 Å).[12] In the trimer, each Mn^{III} is pentacoordinated by two nitrogen and two oxygen atoms from (5,5′-Me_2salen) and one nitrogen atom from cyanide to give a square pyramidal geometry. The Mn–N(5,5′-Me_2salen) (1.971(2)–1.976(2) Å), Mn–O(5,5′-Me_2salen) (1.854(17)–1.878(18) Å) and Mn–N(cyanido) bond lengths (2.165(2) Å) in compound **4** (Table 6) are comparable to those in $[\{Mn(5,5'\text{-}Me_2salen)\}\{Mn(N)(CN)_4\}]$ (Mn–N(5,5′-Me_2salen) 2.004(2) Å, Mn–O(5,5′-Me_2salen) 1.890(19) Å, and Mn-N(cyanido) 2.252(3) Å).[9] The bond lengths in each $[Ru(acac)_2(CN)_2]^-$ unit (Ru1–O = 2.0086(17)–2.0171(16) Å; Ru1–C = 2.060(2) Å; C1–N1 = 1.144(3) Å) are similar to those found in the free *trans*-$[Ru(acac)_2(CN)_2]^-$ anion (Ru2–O = 2.0094(18)-2.0103(18) Å, Ru2–C = 2.067(3) Å, C30–N4 = 1.143(4) Å). The Ru–C≡N angle (177.3(2)°) is close to linear. The free $[Ru(acac)_2(CN)_2]^-$ ions and the methanol molecules are situated between the polymeric chains, leading to a shortest interchain Ru···Ru distance of 11.452 Å. Hydrogen bonding occurs between the free $[Ru(acac)_2(CN)_2]^-$ ion and the two methanol molecules. All of the Ru atoms lie on the twofold axis and the cations stack along the *a* axis (Figure 4, middle and bottom). For each trimer, the Mn···Ru distance is 5.3321(4) Å and the Mn···Mn distance is 10.6642(6) Å, and the Mn···Mn distance between two adjacent trimer units is 3.6244(6) Å.

Magnetic properties

*Compound **1***: The temperature dependence of the magnetic susceptibility of **1** was measured in the range of 2–300 K under an external magnetic field of 1 kOe (Figure 5). The

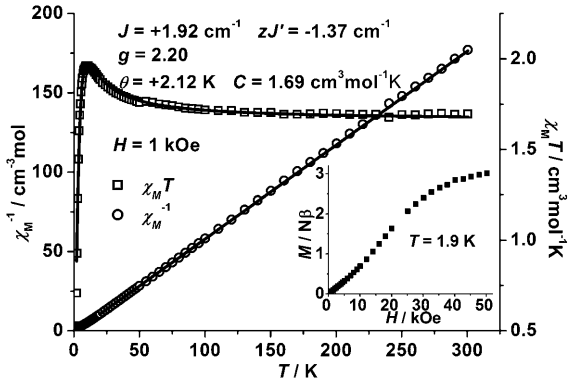

Figure 5. Temperature dependence of $\chi_M T$ (squares) and χ_M^{-1} (circles), and field dependence of the magnetization for compound **1** (inset).

$\chi_M T$ value at room temperature is 1.71 $cm^3 mol^{-1} K$, which is larger than the spin-only value of 1.375 $cm^3 mol^{-1} K$ for one Ni^{II} with $S=1$ and one Ru^{III} center with $S=1/2$, but is consistent with the sum of typical experimental $\chi_M T$ values for one Ni^{II} and one Ru^{III} (the typical $\chi_M T$ value for low-spin Ru^{III} center at room temperature is 0.46 $cm^3 mol^{-1} K$,[5a] larger than the spin-only value due to its orbital contribution). On lowering the temperature, the $\chi_M T$ value increases smoothly and attains a maximum value of 1.96 $cm^3 mol^{-1} K$ at 10 K. It then sharply decreases and reaches a value of 0.708 $cm^3 mol^{-1} K$ at 2.0 K. The molar magnetic susceptibility above 20 K obeys the Curie–Weiss law, $\chi_M = C/(T-\theta)$, with a Curie constant of $C = 1.69\ cm^3 mol^{-1} K$ and a Weiss constant of $\theta = +2.12$ K. The positive θ value and the increasing $\chi_M T$ above 10 K indicates typical ferromagnetic coupling between Ru^{III} and Ni^{II} in **1** through the cyano bridge. The abrupt decrease at lower temperatures may be due to antiferromagnetic interactions between NiRu chains, the saturation effect, and/or the zero-field-splitting effect of the Ni^{II} ions. The magnetization of this compound per [NiRu] unit reaches a value of $3.02 N\beta\ mol^{-1}$ at 2.0 K and 50 kOe (Figure 5 inset), consistent with the expected saturation value of 3.0 $N\beta$ for the sum of one Ru^{III} and one Ni^{II} magnetic moment ($S_T = S_{Ru} + S_{Ni} = 3/2$; $M_S = g S_T N\beta$).

To evaluate the value of the exchange constants of **1**, we used an approximate approach similar to that for 1D, 2D, and quasi-2D complexes.[13] The cyanide bridges between Ni^{II} and Ru^{III} were regarded equal, since the bridging modes through C1N1 and C2N2 were almost the same. Therefore, the 1D chain can be treated as alternating uniform NiRu dimers with the exchange constant J and interchain interactions zJ'. For an asymmetrical $Ni^{II}Ru^{III}$ dinuclear compound with $S_{Ni}=1$ and $S_{Ru}=1/2$, we regard the g tensors as equal. The spin Hamiltonian is given by Equation (1). Thus the molar magnetic susceptibility of the dimer[14] can be expressed as given in Equation (2). Also the molar magnetic susceptibility of the dimer is written as in Equation (3). Then the chain magnetic susceptibility is as shown in Equation (4), in which $u = \coth(JS_d(S_d+1)/kT) - kT/JS_d(S_d+1)$. Furthermore, based on the molecular field theory, the fit function can be modified to include the inter-

chain coupling as shown in Equation (5), in which J' is the interchain exchange coupling constant and z is the number of the nearest neighbor chains. The best fitting in the temperature range of 2–300 K gives $J=+1.92\,cm^{-1}$, $zJ'=-1.37\,cm^{-1}$, $g=2.20$ with $R=3.21\times10^{-4}$ ($R=\Sigma[(\chi_M T)_{obs}-(\chi_M T)_{calcd}]^2/\Sigma(\chi_M T)_{obs}^2$). The positive value of exchange coupling through the cyanide bridges suggests ferromagnetic interactions between Ni^{II} and Ru^{III} centers, and the relatively large negative value of zJ' indicates obvious antiferromagnetic interactions between the neighboring $Ni^{II}Ru^{III}$ chains, which result in the sharp decrease of $\chi_M T$ value below 10 K.

$$H=-2JS_{Ni}S_{Ru}+\beta(S_{Ni}S_{Ni}+S_{Ru}S_{Ru})H \quad (1)$$

$$\chi_d=\frac{Ng^2\beta^2}{4kT}\frac{1+\frac{1}{10}\exp(3J/kT)}{1+2\exp(3J/kT)} \quad (2)$$

$$\chi_d=\frac{Ng^2\beta^2}{3kT}S_d(S_d+1) \quad (3)$$

$$\chi_c=\frac{Ng^2\beta^2}{3kT}\frac{1+u}{1-u}S_d(S_d+1) \quad (4)$$

$$\chi=\frac{\chi_c}{1-(2zJ'/Ng^2\beta^2)\chi_c} \quad (5)$$

Compound ***2***: The magnetic properties of **2** were measured at a field of 1 kOe in the range of 2–300 K (Figure 6). The $\chi_M T$ value at room temperature is $1.70\,cm^3mol^{-1}K$, similar to compound **1**, which is larger than the spin-only value of $1.375\,cm^3mol^{-1}K$ for one Ni^{II} ($S=1$) and one Ru^{III} ($S=1/2$), but is consistent with the sum of typical experimental $\chi_M T$ values for one Ni^{II} and one Ru^{III}. Upon lowering the temperature, the $\chi_M T$ value increases smoothly and attains a maximum value of $4.19\,cm^3mol^{-1}K$ at 2 K. Fitting the data above 50 K with the Curie–Weiss law [$\chi_M=C/(T-\theta)$] gives $C=1.67\,cm^3mol^{-1}K$ and $\theta=+4.50$ K. The positive θ value indicates ferromagnetic interaction between Ru^{III} and Ni^{II} through the cyanide bridge, which is expected from the orthogonality of the magnetic orbitals of the metal ions. The magnetization of this compound per [NiRu] unit reaches a value of 3.25 $N\beta$ mol^{-1} at 2.0 K and 50 kOe (Figure 6 inset), nearly consistent with the expected saturation value of 3.0 $N\beta$ for the sum of one Ru^{III} and one Ni^{II} magnetic moment. Using a similar model as that for compound **1**, the susceptibility from 2 to 300 K were simulated, giving the best fit with parameters $J=+0.85\,cm^{-1}$, $zJ'=-0.16\,cm^{-1}$ and $g=2.24$ with $R=7.92\times10^{-4}$. These results indicate ferromagnetic interactions between Ni^{II} and Ru^{III} centers. Thus, compound **2** can be viewed as a regular chain with only one kind of magnetic coupling.

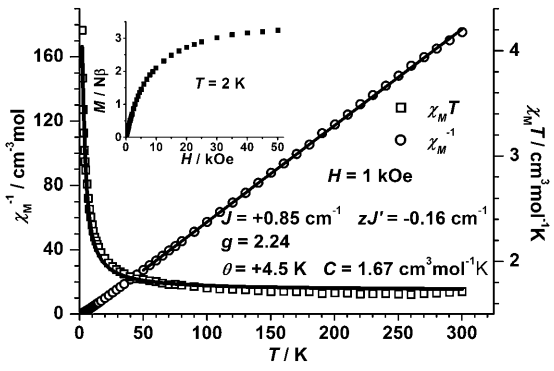

Figure 6. Temperature dependence of $\chi_M T$ (squares) and χ_M^{-1} (circles), and field dependence of the magnetization for compound **2** (inset).

Compound ***3***: The temperature dependence of the magnetic susceptibility for compound **3** measured in the temperature range of 2–300 K under the external magnetic field of 1 kOe is illustrated in Figure 7. The $\chi_M T$ value at room temperature is $5.32\,cm^3mol^{-1}K$, which is slightly larger than the spin-only value of $4.75\,cm^3mol^{-1}K$ for one high-spin Fe^{III} center in octahedral symmetry with $S=5/2$ and one low-spin d^5 Ru^{III} center in octahedral symmetry with $S=1/2$. On lowering the temperature, the $\chi_M T$ value increases smoothly and attains a maximum value of $13.11\,cm^3mol^{-1}K$ at 3.0 K and then it decreases sharply and reaches a value of $5.90\,cm^3mol^{-1}K$ at 2.0 K. The χ_M values above 50 K obey the Curie–Weiss law [$\chi_M=C/(T-\theta)$] with $C=5.14\,cm^3mol^{-1}K$ and $\theta=+4.90$ K. The large C value and the positive θ suggest ferromagnetic coupling between Ru^{III} and Fe^{III} through the cyanide bridge.

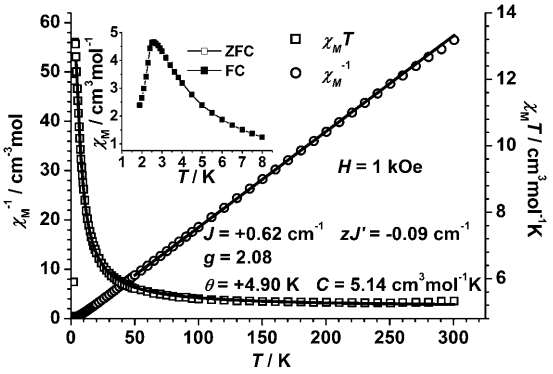

Figure 7. Temperature dependence of $\chi_M T$ (squares) and χ_M^{-1} (circles) for compound **3**. Inset: Plots of ZFC and FC magnetization at 20 Oe.

On the basis of the dimeric model similar to compound **1**, the magnetic susceptibility of the $Ru^{III}Fe^{III}$ dimer can be expressed by Equation (6)[15] derived from the isotropic exchange spin Hamiltonian $H=-2JS_AS_B$. Through the same processing method as compound **1**, the susceptibilities from 4 to 300 K were simulated giving the best fit with parameters $J=+0.62\,cm^{-1}$, $zJ'=-0.09\,cm^{-1}$ and $g=2.08$ with $R=3.06\times10^{-5}$. The plots of the zero-field cooled (ZFC) and field-cooled (FC) $\chi_M(T)$ at 20 Oe (Figure 7 inset) clearly show a transition from ferromagnetic to antiferromagnetic behavior at about 2.6 K.

$$\chi_d = \frac{Ng^2\beta^2}{kT}\frac{10\exp(-3J/kT)+28}{5\exp(-3J/kT)+7} \quad (6)$$

The metamagnetic behavior was further characterized by the measurement of field-dependent magnetization at 1.9 K. Figure 8 (upper inset) shows that the curve has the sigmoidal shape expected for a metamagnet; the magnetization first increases slowly with the external field because of antiferromagnetic interchain interactions and then increases sharply, showing a phase transition to a ferromagnetic state. When the field is increased further, the magnetization reaches a saturation magnetization of $6.30N\beta$ (expected value: $6.0N\beta$ for $S_T=3$) at 50 kOe.

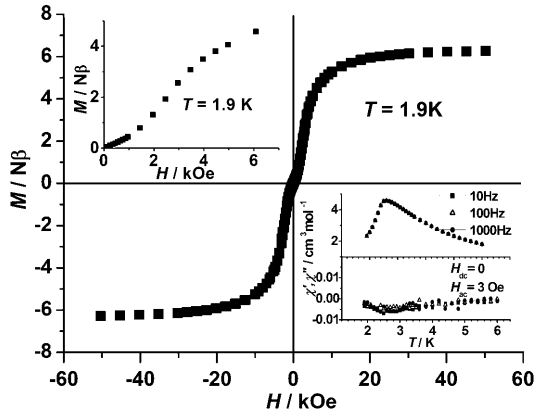

Figure 8. Hysteresis loop at 1.9 K for **3**. Inset (upper): Field dependence of the magnetization; (lower): Temperature dependence of the real (χ') and imaginary (χ'') parts of the ac susceptibility measured at $H_{dc}=0$ under various oscillating frequencies (10, 100, 1000 Hz).

A hysteresis loop at 1.9 K (Figure 8) was observed with a very small coercive field, typical of a soft magnet. The "double-S" shape of the curve is indicative of a metamagnet, which switches from an antiferromagnetic ground state to a ferromagnetic-like state upon the application of a large enough field. The magnetic phase transition is further confirmed by the temperature dependence at zero dc and 3 Oe ac field. The field susceptibility measurements are displayed in Figure 8 (lower inset). The real part (χ') of the ac magnetic susceptibility has a maximum at about 2.6 K for frequencies of 10, 100, and 1000 Hz, and the imaginary part (χ'') is negligibly small, suggesting antiferromagnetic ordering below 2.6 K.

Compound ***4***: The temperature dependence of the magnetic susceptibility for compound **4** measured in the temperature range of 2–300 K under an external magnetic field of 1 kOe is illustrated in Figure 9. The $\chi_M T$ value at 300 K is 6.92 $cm^3 mol^{-1} K$, which is larger than the uncoupled, spin-only value of 6.375 $cm^3 mol^{-1} K$ for two high-spin Mn^{III} centers in a square pyramidal symmetry with $S=2$ and one low-spin d^5 Ru^{III} center in an octahedral symmetry with $S=1/2$,

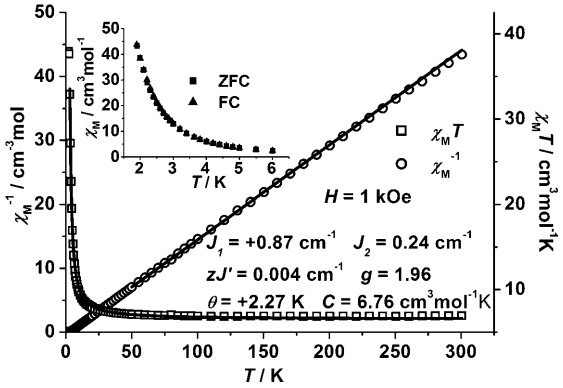

Figure 9. Temperature dependence of $\chi_M T$ (squares) and χ_M^{-1} (circles) for compound **4**. The inset is plots of ZFC and FC magnetization at 20 Oe for **4**.

due to their orbital contributions. On lowering the temperature, the $\chi_M T$ value remains nearly constant until 75 K, it then increases rapidly and attains a value of 37.92 $cm^3 mol^{-1} K$ at 2.0 K. The molar magnetic susceptibility data of compound **4** can be fitted using the Curie–Weiss law $[\chi_M = C/(T-\theta)]$ above 50 K, giving $C=6.76$ $cm^3 mol^{-1} K$ and $\theta=+2.27$ K. The positive θ value and the increase in $\chi_M T$ on lowering the temperature are typical of ferromagnetic coupling between Ru^{III} and Mn^{III} in **4** through the cyanide bridge. The ZFC/FC plot (Figure 9 inset) does not show a divergence above 2 K, indicating long-range ordering does not occur above 2 K.

On the basis of the structural description, two different exchange couplings can be identified along the chain: 1) a $Mn^{III}\cdots Ru^{III}$ interaction, J_1, through a cyano bridge; and 2) a $Mn^{III}\cdots Mn^{III}$ exchange, J_2, through π–π interactions. Here, a Heisenberg trinuclear model was used to simulate the magnetic susceptibility with the spin system (S_{Mn}, S_{Ru}, $S_{Mn}=2$, $^1/_2$, 2) similar to the compound $[NEt_4][Mn_2(5\text{-MeOsalen})_2Fe(CN)_6]$.[12] A Heisenberg Hamiltonian [Eq. (7)] was used assuming an external magnetic field (H) along the z axis, in which S_T is the total spin operator of the trimer with $S_T = S_{Mn1} + S_{Ru} + S_{Mn1A}$; S_{Tz} is the z component of the S_T operator, and g is the Landé factor assuming $g=g_{Mn}=g_{Ru}$. In the low-field limit, an analytical expression of the susceptibility can be obtained [Eq. (8)]. Also the molar magnetic susceptibility of the trimer is written according to Equation (9). Then the magnetic susceptibility of **4** is as given in Equation (10), in which $u = \coth(J_2S_t(S_t+1)/kT) - kT/J_2S_t(S_t+1)$.

$$H = -2J(S_{Mn1}S_{Ru} + S_{Mn1A}S_{Ru}) + gN\beta S_{Tz}H_z \quad (7)$$

$$\chi_t = \frac{Ng^2\beta^2}{4kT}\frac{(e^{\frac{-3J_1}{kT}}+e^{\frac{-4J_1}{kT}})+10(e^{\frac{-7J_1}{kT}}+e^{\frac{-3J_1}{kT}})+35(e^{\frac{-8J_1}{kT}}+e^{\frac{-2J_1}{kT}})+84(e^{\frac{-9J_1}{kT}}+e^{\frac{-J_1}{kT}})+165}{(e^{\frac{-3J_1}{kT}}+e^{\frac{-4J_1}{kT}})+2(e^{\frac{-7J_1}{kT}}+e^{\frac{-3J_1}{kT}})+3(e^{\frac{-8J_1}{kT}}+e^{\frac{-2J_1}{kT}})+4(e^{\frac{-9J_1}{kT}}+e^{\frac{-J_1}{kT}})+5} \quad (8)$$

$$\chi_t = \frac{Ng^2\beta^2}{3kT}S_t(S_t+1) \quad (9)$$

$$\chi_c = \frac{Ng^2\beta^2}{3kT}\frac{1+u}{1-u}S_t(S_t+1) + \frac{Ng^2\beta^2}{3kT}S_{Ru}(S_{Ru}+1) \quad (10)$$

The inter-trimer interaction, J', was introduced in the frame of the mean field approximation. The fit function can be modified to include the interchain coupling [Eq. (11)], in which J' is the interchain exchange coupling constant and z is the number of the nearest neighbor chains. The magnetic data in range of 3-300 K were fitted, giving the best result with the parameters $J_1 = +0.87\ cm^{-1}$, $J_2 = +0.24\ cm^{-1}$, $zJ' = +0.004\ cm^{-1}$ and $g = 1.96$ with $R = 7.51 \times 10^{-4}$. It should be noted that the anisotropy of the system was neglected in the magnetic model, and, therefore, the magnetic interaction values, especially J', could be slightly changed if this contribution is taken into account.

$$\chi = \frac{\chi_c}{1 - (2zJ'/Ng^2\beta^2)\chi_c} \quad (11)$$

The rapid rise in M with H at 1.9 K confirms the overall intermolecular ferromagnetic coupling. At the highest measured field (50 kOe), the magnetization of this compound reaches a value of 7.72 $N\beta$ mol^{-1} (Figure 10 inset), indicating

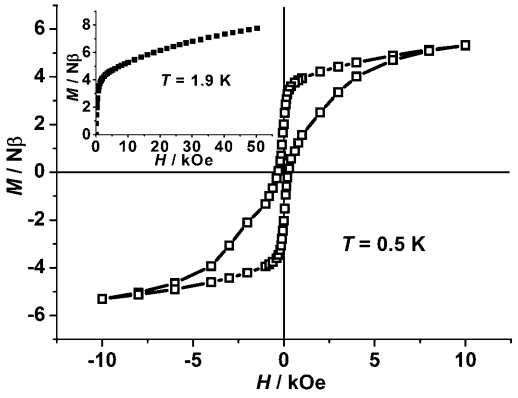

Figure 10. Hysteresis loop at 0.5 K for **4**. Inset: field dependence of the magnetization.

that saturation (expected value of 9.0 $N\beta$ for $S_T = S_{Ru} + 2S_{Mn} = 9/2$; $M_s = gS_TN\beta$) has not yet been achieved. Such behavior can be often observed in $[Mn(SB)]^+$-containing compounds (SB = Schiff Base)[16] because of the large zero-field splitting of Mn^{III} ions. A hysteresis loop is observed at 0.5 K (Figure 10) with values of the coercive field (H_c) and remnant magnetization (M_r) of about 300 Oe and 2.0 $N\beta$, respectively.

To probe the magnetization dynamics of **4**, ac susceptibility measurements were performed in a 3 Oe oscillating field with a zero dc field from 10 to 1000 Hz. The in-phase (χ') and out-of-phase (χ'') signals show apparent frequency dependency (Figure 11). The maxima of χ' and χ'' shift to high temperature when the frequency of the oscillating field is increased, confirming the slow relaxation of the magnetization. The blocking of the magnetization below 2.2 K is not

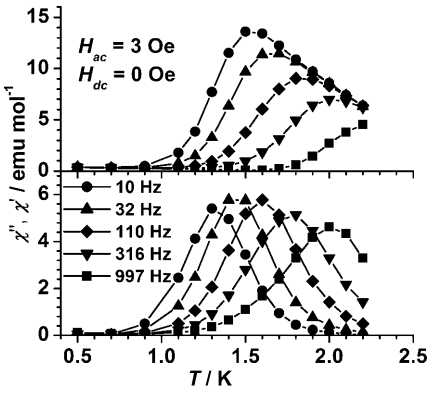

Figure 11. Temperature dependence of the real (χ') and imaginary (χ'') parts of the ac susceptibility for **4** measured under various oscillating frequencies (10–1000 Hz) with zero field.

due to a phase transition to a 3D order or a spin glass, according to ac magnetic susceptibility measurements. The shift of peak temperature (T_P) of the in phase signal χ' is measured by a parameter $\phi = (\Delta T_p/T_p)/\Delta \log f = 0.25$, which is two orders of magnitude larger than that for a canonical spin glass, but is in excellent agreement with that expected for superparamagnetic behavior and excludes the possibility of a spin glass. From the data shown in Figure 11, the relaxation time τ, can be determined from the maximum of $\chi''(T)$.[17] The relaxation time for **4** follows an Arrhenius law with an energy gap of 16.4 K and $\tau_0 = 3.04 \times 10^{-7}$ s (Figure 12).

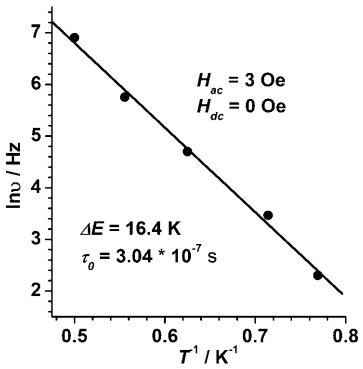

Figure 12. The plot of lnυ versus T^{-1} for **4**.

The magnetic behavior of **4** could be attributed to the unique 1D supramolecular organization through the π–π stacking. The Mn···Mn distance through the π–π stacking is only 3.624 Å, similar to the separation through a single atom bridging mode. The free $[Ru(acac)_2(CN)_2]^-$ ions separate the polymeric chains and thus weaken the interchain interaction, which is consistent with the very small zJ' value. The slow magnetic relaxation reflects that the contributions to the energy barrier come from both the anisotropy of isolated cluster and intercluster interactions. Compound **4** behaves as an unusual single-chain magnet rather than as a single-molecule magnet due to the strong interaction be-

tween the clusters in the chain through noncovalent stacking.

DFT calculations: Based on previous work on the application of the DFT+BS method in the calculation of the magnetic coupling of transition metal complexes,[5b,18] the structures of the 1D compounds **1**, **3**, and **4** are simplified to one dimer model, Frag **1**, and two trimer models, Frag **3** and Frag **4**, respectively, which are depicted in Figure 13. The magnetic coupling constant J between Ru^{III} and the 3d ions could be evaluated using the Heisenberg spin Hamiltonian: $H=-2J\Sigma S_i \cdot S_j$ and energies of high- and low-spin states. The details of calculations have been described elsewhere.[5b]

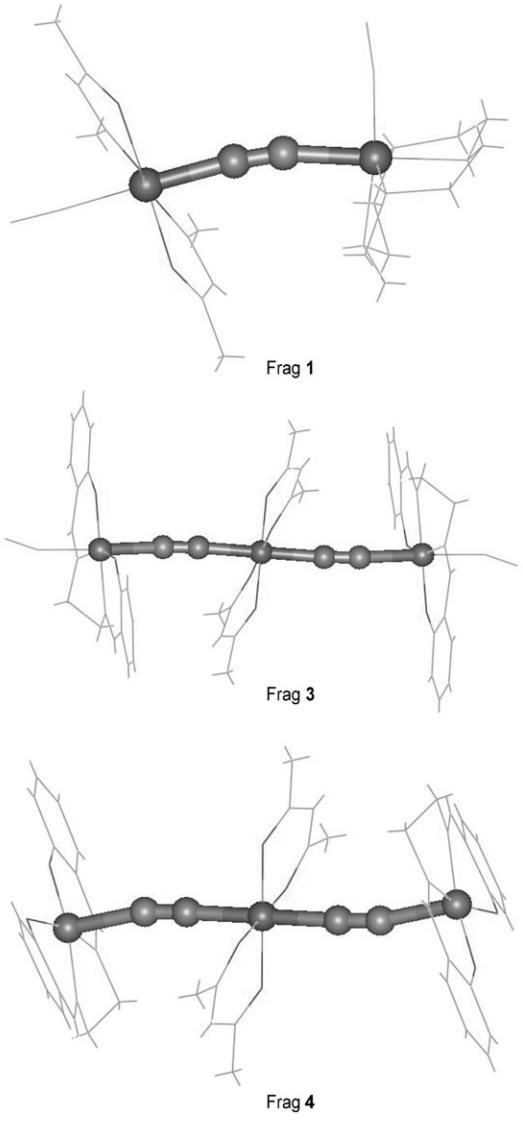

Figure 13. Model molecular structures for Ru–Ni compound **1** (Frag **1**); Ru–Fe compound **3** (Frag **3**) and Ru–Mn compound **4** (Frag **4**).

The calculated J between Ru^{III} and Ni^{II} ions of Frag **1** is 5.4 cm^{-1}, which is consistent with the experimental results and indicates that ferromagnetic coupling is transmitted by the cyano bridge. Considering the ligand field of octahedral symmetry surrounding Ru^{III} and Ni^{II} ions, the spin unpaired electrons are located in the t_{2g} orbitals of Ru^{III} and the e_g orbitals of Ni^{II} ions. From Kahn's model, ferromagnetic coupling between spin electrons located in orthogonal orbitals is a theoretically expected property.[14] Julve et al. also discussed the weak ferromagnetic coupling in Ru–Ni systems, which was attributed to the inappropriate orientation of the magnetic orbital of the low-spin ruthenium(III) compared with nickel(II).[5d]

The calculated J_{Ru-Fe} value of the Fe–Ru–Fe trimer (Frag **3**) is 6.4 cm^{-1}, which is also consistent with the experimental result. The calculated J_{Fe-Fe} of the trimer is -0.14 cm^{-1}, which is much smaller than J_{Ru-Fe}. This supports that ignoring J_{Fe-Fe} is reasonable for the magnetic data fitting process for compound **3**. In the Fe–Ru–Fe trimer, antiferromagnetic coupling (AF) of the spin unpaired electrons in the t_{2g} orbitals of Ru^{III} and Fe^{III}, and ferromagnetic coupling (F) between the spin unpaired electrons in orthogonal t_{2g} orbitals of Ru^{III} and e_g orbitals of Fe^{III} are both present. Usually when both AF and F contributions are present, AF contribution dominates and the overall interaction is AF.[2] Hence, the observed ferromagnetic coupling between the low-spin Ru^{III} ion and the high-spin Fe^{III} ion in the Fe–Ru–Fe trimer is somewhat unexpected. A detailed analysis of the magnetic orbitals shows that the main exchange pathway is the antibonding orbital composed of the d_{xz} orbital of Ru^{III}, the d_{z^2} orbital of Fe^{III} and the p orbital of CN ligand; which is depicted in Figure 14. These two orthogonal atomic orbital

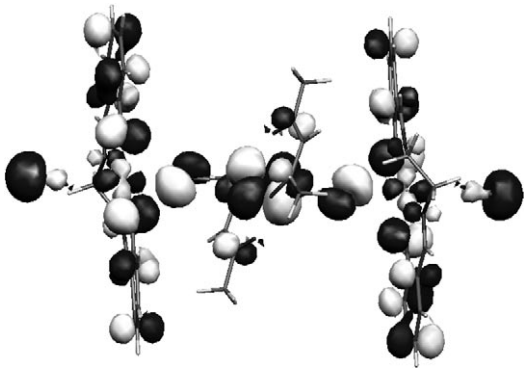

Figure 14. Selected molecular magnetic orbital for Ru–Fe compound **3**.

components contribute to ferromagnetic coupling. But why do the t_{2g} orbitals of Ru^{III} and Fe^{III} not overlap efficiently with each other to produce antiferromagnetic coupling? A clue to solving this puzzle may be obtained by examining the energy spectrum of the single nuclear model from compound **3** produced by DFT calculations. The average t_{2g} orbital energy of Ru^{III} is 3.54 eV higher than the corresponding t_{2g} orbital energy of Fe^{III}, but only 0.15 eV higher than the average e_g orbital energy of Fe^{III}. From the point of view of orbital energy matching, the interaction between orthogonal t_{2g} orbital of Ru^{III} and e_g orbital of Fe^{III} should dominate

in the Ru–Fe compound, resulting in overall ferromagnetic coupling. Based on the analysis above, it seems that apart from the relative symmetries, the relative energies of the magnetic orbitals may also be important in determining the overall magnetic coupling in bimetallic assemblies, especially for 3d–4d, and possible also 3d–5d assemblies. In the compound $[Bu_4N][Fe^{II}Ru^{III}(ox)_3]$, which has a 2D oxalate-bridged structure, the Ru^{III}–Fe^{II} interactions are AF.[7] Also in our previously reported trimer $[\{Mn(CH_3OH)_4\}\{Ru(salen)(CN)_2\}_2]\cdot 6CH_3OH\cdot 2H_2O$ and 2D $\{Mn(H_2O)_2[Ru(salen)(CN)_2]_2\cdot H_2O\}_n$, AF interactions between Ru^{III} and Mn^{II} are observed for both compounds.[5b] Presumably in these compounds the t_{2g} orbital energies of Ru^{III} and M^{II} are comparable so that AF interaction dominates. Hence, for M^NRu^{III} assemblies, it may be possible to tune the magnetic interaction between M^N and Ru^{III} by changing the ligands on M and Ru and/or the oxidation state of M.

For the Mn–Ru–Mn trimer model compound, the initial calculated coupling constant J_{Ru-Mn} between Ru^{III} and Mn^{III} is 7.9 cm^{-1}, which is also ferromagnetic but is much higher than the experimental value of 0.87 cm^{-1}. To obtain more precise energies of high-spin and broken symmetry states, the post-SCF (SCF = self-consistent field) energies of the system with hybrid O3LYP[19] functionals are also used in the calculations. The final calculated J_{Ru-Mn} value is 1.4 cm^{-1}, which agrees better with the experimental result. As in the case of the Fe–Ru–Fe trimer described above, the observed ferromagnetic coupling is also somewhat unexpected, but may also be rationalized by using a similar analysis as the Fe–Ru–Fe trimer.

Conclusion

A series of $Ru^{III}M^{II/III}$ (M = Ni^{II}, Fe^{III}, Mn^{III}) bimetallic chains were synthesized from *trans*-$[Ru^{III}(acac)_2(CN)_2]^-$ and ML^{n+} (L = ancilliary ligand). The bond lengths and bond angles of $[Ru(acac)_2(CN)_2]^-$ and ML^{n+} units in these compounds are similar to that of the free ions, indicating that a change in oxidation states of Ru and M did not occur in the formation of the bimetallic chains. The $\chi_M T$ values of the compounds at room temperature are also consistent with the presence of Ru^{III} and M. These compounds all exhibit intrachain ferromagnetic coupling between Ru^{III} and $M^{II/III}$ through cyanide ligands. Compounds **1** and **2** consist of zigzagged $Ru^{III}Ni^{II}$ chains. Compound **3** consists of linear $Ru^{III}Fe^{III}$ chains, and it exhibits metamagnetic behavior with $T_N = 2.6$ K. Compound **4** is a novel single-chain magnet built from Mn_2Ru trimers linked together by noncovalent interactions. DFT calculations suggest that apart from the relative symmetries, the relative energies of the magnetic orbitals are also important in determining the overall magnetic properties of the compounds. The energies of the magnetic orbitals may be tuned by varying the ancilliary ligands and the oxidation states of the metal centers. These findings may provide insight in designing 3d–4d or 3d–5d materials with desirable magnetic properties.

Experimental Section

Materials and reagents: All chemicals and solvents were of reagent grade and used as received. *trans*-$Ph_4P[Ru(acac)_2(CN)_2]$,[5a] [Fe(salen)(OAc)][20] and $[Mn(5,5'\text{-}Me_2salen)]PF_6$[21] were synthesized by literature methods. $[Ni(tren)][ClO_4]_2$ and $[Ni(cyclen)][ClO_4]_2$ were prepared by mixing a methanol solution of $Ni(ClO_4)_2\cdot 6H_2O$ with a methanol solution of tren or cyclen.

Synthesis

$[\{Ni(tren)\}\{Ru(acac)_2(CN)_2\}][ClO_4]\cdot CH_3OH$ (1): X-ray quality crystals of **1** were grown in a CH_3OH/DMF (9:1 v/v) mixture by slow diffusion in an H-shaped tube with *trans*-$Ph_4P[Ru(acac)_2(CN)_2]$ (40 mg, 0.058 mmol) at one arm and $[Ni(tren)](ClO_4)_2$ (23 mg, 0.058 mmol) at the other. Red plate crystals of **1** were formed on standing at room temperature for three days. Yield: 24 mg (61.5%). IR (KBr): $\tilde{\nu} = 2137\ cm^{-1}$ (C≡N); elemental analysis calcd (%) for $C_{18}H_{34}ClN_6NiO_9Ru$: C 32.08, H 5.08, N 12.47; found: C 31.85, H 5.02, N 12.43.

$[\{Ni(cyclen)\}\{Ru(acac)_2(CN)_2\}](ClO_4)\cdot CH_3OH$ (2): $[Ni(cyclen)](ClO_4)_2$ (25 mg, 0.058 mmol) was dissolved in DMF (3 mL) in a test tube. *trans*-$Ph_4P[Ru(acac)_2(CN)_2]$ (40 mg, 0.058 mmol) dissolved in methanol (5 mL) was carefully layered above the DMF solution. Well defined dark red block crystals were obtained after leaving the test tube undisturbed at room temperature for about one week. Yield: 21 mg (50.7%). IR (KBr): $\tilde{\nu} = 2133\ cm^{-1}$ (C≡N); elemental analysis calcd (%) for $C_{21}H_{38}ClN_6NiO_9Ru$: C 35.34, H 5.37, N 11.77; found: C 35.45, H 5.42, N 11.81.

$[\{Fe(salen)\}\{Ru(acac)_2(CN)_2\}]$ (3): *trans*-$Ph_4P[Ru(acac)_2(CN)_2]$ (40 mg, 0.058 mmol) in methanol (5 mL) was added to a solution of [Fe(salen)(OAc)] (22.1 mg, 0.058 mmol) in methanol (5 mL) . Well-defined dark plate crystals were obtained by slow evaporation of the resulting solution at room temperature for one week. Yield: 22 mg (55.6%). IR (KBr): $\tilde{\nu} = 2118\ cm^{-1}$ (C≡N); elemental analysis calcd (%) for $C_{28}H_{28}FeN_4O_6Ru$: C 49.94, H 4.19, N 8.32; found: C 49.83, H 4.50, N 8.27.

$[\{Mn(5,5'\text{-}Me_2salen)\}_2\{Ru(acac)_2(CN)_2\}][Ru(acac)_2(CN)_2]\cdot 2CH_3OH$ (4): *trans*-$Ph_4P[Ru(acac)_2(CN)_2]$ (30 mg, 0.043 mmol) and $[Mn(5,5'\text{-}Me_2salen)]PF_6$ (21.2 mg, 0.043 mmol) were dissolved in a minimum volume of methanol. After about 5 h, the mixture was filtered to remove PPh_4PF_6. Dark red block crystals suitable for X-ray crystallography were obtained by slow evaporation of the filtrate at room temperature for 3 days. Yield: 20 mg (65.0%). IR (KBr): $\tilde{\nu} = 2120, 2090\ cm^{-1}$ (C≡N); elemental analysis calcd (%) for $C_{60}H_{64}Mn_2N_8O_{12}Ru_2$: C 51.06, H 4.61, N 7.94; found: C 50.98, H 4.94, N 7.93.

Caution! Perchlorate salts of metal complexes with organic ligands are potentially explosive and should be handled in small quantities with care.

Physical measurements: Elemental analyses of all the compounds were performed on an Elementar vario EL III carbon hydrogen nitrogen analyzer. IR spectra were recorded on a Nicolet 360 spectrophotometer with KBr pellets in the 400–4000 cm^{-1} region.

X-ray crystallography: All measurements were recorded on a Bruker SMART CCD diffractometer with graphite-monochromated $Mo_{K\alpha}$ radiation ($\lambda = 0.71073$ Å). The structures were solved by direct methods (SHELXS97)[22] and expanded using Fourier techniques. All non-hydrogen atoms were refined anisotropically. All H-atoms were refined using riding model with $U_{iso}(H) = 1.2\,U_{eq}$(Carrier).

CCDC-736358 (**1**), CCDC-736359 (**2**), CCDC-736360 (**3**) and CCDC-736361 (**4**) contain the supplementary crystallographic data for this paper. These data can be obtained free of charge from The Cambridge Crystallographic Data Centre via www.ccdc.cam.ac.uk/data_request/cif.

Magnetic measurements: Variable-temperature magnetic susceptibility, ac magnetic susceptibility, and field dependence of magnetization were measured on a Quantum Design MPMS XL-5 SQUID system. Background corrections were done by experimental measurement on the sample holder. The experimental susceptibilities were corrected for the diamagnetism of the constituent atoms (Pascal's tables).

Computational methods: The density functional theory (DFT) method combined with the broken symmetry approach (BS) was used to calculate

the magnetic exchange interaction between Ru^{III} and 3d ions; including Ni^{II}, Fe^{III}, and Mn^{III} ions. All theoretical calculations were performed by using the Amsterdam density functional (ADF) package, version 2007.01.[23] Both the local density approximation (LDA) and the generalized gradient approximation (GGA) were used, including the scaled ZORA relativistic correction. The VWN5[24] functionals at LDA level and the mPW[25] exchange and correlation functionals at GGA level were applied for solving the Kohn–Sham equation. The frozen core approximation for the inner core electrons was used for all non-hydrogen atoms. The orbital shells up to 3d for Ru; up to 2p for Fe, Mn and Ni; and up to 1s for C, N, O were kept frozen. The valence electrons were described with triple-ς valence plus polarization basis sets (TZP). All the functionals and basis sets in this work have been tested in another theoretical computation,[18] so they were used directly without further comparison studies.

Acknowledgements

The work described in this paper was supported by grants from the National Natural Science Foundation of China (20831160505), the National Basic Research Program of China (2009CB929403), the Research Grants Council of Hong Kong Joint Research Scheme (N CityU 107/08), and the City University of Hong Kong (SRG 7002095). We thank Prof. Z. D. Chen and S. D. Jiang for helpful discussions.

[1] a) T. Mallah, S. Thiébault, M. Verdaguer, P. Veillet, *Science* **1993**, *262*, 1554–1557; b) S. Ferlay, T. Mallah, R. Ouhaès, P. Veillet, M. Verdaguer, *Nature* **1995**, *378*, 701–703; c) R. Garde, F. Villain, M. Verdaguer, *J. Am. Chem. Soc.* **2002**, *124*, 10531–10538; d) S. M. Holmes, G. S. Girolami, *J. Am. Chem. Soc.* **1999**, *121*, 5593–5594; e) Ø. Hatlevik, W. E. Buschmann, J. Zhang, J. L. Manson, J. S. Miller, *Adv. Mater.* **1999**, *11*, 914–918; f) S. Ohkoshi, M. Mizuno, G. J. Hung, K. Hashimoto, *J. Phys. Chem. B* **2000**, *104*, 9365–9367.

[2] M. Verdaguer, A. Bleuzen, V. Marvaud, J. Vaissermann, M. Seuleiman, C. Desplanches, A. Scuiller, C. Train, R. Garde, G. Gelly, C. Lomenech, I. Rosenman, P. Veillet, C. Cartier, F. Villain, *Coord. Chem. Rev.* **1999**, *190–192*, 1023–1047.

[3] a) J. J. Sokol, A. G. Hee, J. R. Long, *J. Am. Chem. Soc.* **2002**, *124*, 7656–7657; b) D. Li, S. Parkin, G. Wang, G. T. Yee, A. V. Prosvirin, S. M. Holmes, *Inorg. Chem.* **2005**, *44*, 4903–4905; c) S. Wang, J.-L. Zou, H. C. Zhou, H. J. Choi, Y. Ke, J. R. Long, X.-Z. You, *Angew. Chem.* **2004**, *116*, 6066–6069; *Angew. Chem. Int. Ed.* **2004**, *43*, 5940–5943; d) E. J. Schelter, A. V. Prosvirin, K. R. Dunbar, *J. Am. Chem. Soc.* **2004**, *126*, 15004–15005; e) D. Li, S. Parkin, G. Wang, G. T. Yee, R. Clérac, W. Wernsdorfer, S. M. Holmes, *J. Am. Chem. Soc.* **2006**, *128*, 4214–4215; f) D. Li, R. Clérac, G. Wang, G. T. Yee, S. M. Holmes, *Eur. J. Inorg. Chem.* **2007**, 1341–1346; g) D. Li, R. Clérac, S. Parkin, G. T. Yee, S. M. Holmes, *Inorg. Chem.* **2006**, *45*, 5251–5253; h) D. Li, R. Clérac, S. Parkin, G. Wang, G. T. Yee, S. M. Holmes, *Inorg. Chem.* **2006**, *45*, 7569–7571.

[4] a) R. Lescouëzec, J. Vaissermann, C. Ruiz-Pérez, F. Lloret, R. Carrasco, M. Julve, M. Verdaguer, Y. Dromzee, D. Gatteschi, W. Wernsdorfer, *Angew. Chem.* **2003**, *115*, 1521–1524; *Angew. Chem. Int. Ed.* **2003**, *42*, 1483–1486; b) L. M. Toma, R. Lescouëzec, F. Lloret, M. Julve, J. Vaissermann, M. Verdaguer, *Chem. Commun.* **2003**, 1850–1851; c) S. Wang, J. L. Zuo, S. Gao, Y. Song, H. C. Zhou, Y. Z. Zhang, X. Z. You, *J. Am. Chem. Soc.* **2004**, *126*, 8900–8901; d) L. M. Toma, R. Lescouëzec, J. Pasán, C. Ruiz-Pérez, J. Vaissermann, J. Cano, R. Carrasco, W. Wernsdorfer, F. Lloret, M. Julve, *J. Am. Chem. Soc.* **2006**, *128*, 4842–4853; e) H. R. Wen, C. F. Wang, Y. Song, S. Gao, J. L. Zuo, X. Z. You, *Inorg. Chem.* **2006**, *45*, 8942–8949; f) L. M. Toma, R. Lescouëzec, S. Uriel, R. Llusar, C. Ruiz-Pérez, J. Vaissermann, F. Lloret, M. Julve, *Dalton Trans.* **2007**, 3690–3698; g) D. Visinescu, L. M. Toma, F. Lloret, O. Fabelo, C. Ruiz-Pérez, M. Julve, *Dalton Trans.* **2008**, 4103–4105; h) H. Miyasaka, M. Julve, M. Yamashita, R. Clérac, *Inorg. Chem.* **2009**, *48*, 3420–3437.

[5] a) W. F. Yeung, W. L. Man, W. T. Wong, T. C. Lau, S. Gao, *Angew. Chem.* **2001**, *113*, 3121–3123; *Angew. Chem. Int. Ed.* **2001**, *40*, 3031–3033; b) W. F. Yeung, P. H. Lau, T. C. Lau, H. Y. Wei, H. L. Sun, S. Gao, Z. D. Chen, W. T. Wong, *Inorg. Chem.* **2005**, *44*, 6579–6590; c) W. F. Yeung, T. C. Lau, X. Y. Wang, S. Gao, L. Szeto, W. T. Wong, *Inorg. Chem.* **2006**, *45*, 6756–6760; d) L. M. Toma, L. D. Toma, F. S. Delgado, C. Ruiz-Pérez, J. Sletten, J. Canod, J. M. Clemente-Juan, F. Lloret, M. Julve, *Coord. Chem. Rev.* **2006**, *250*, 2176–2193; e) J. A. Duimstra, C. L. Stern, T. J. Meade, *Polyhedron* **2006**, *25*, 2705–2709; f) J. H. Yoon, H. S. Yoo, H. C. Kim, S. W. Yoon, B. J. Suh, C. S. Hong, *Inorg. Chem.* **2009**, *48*, 816–818.

[6] F. M. Crean, K. Schug, *Inorg. Chem.* **1984**, *23*, 853–857.

[7] J. Larionova, B. Mombelli, J. Sanchiz, O. Kahn, *Inorg. Chem.* **1998**, *37*, 679–684.

[8] M. S. El Fallah, E. Rentschler, A. Caneschi, R. Sessoli, D. Gatteschi, *Angew. Chem.* **1996**, *108*, 2081–2083; *Angew. Chem. Int. Ed. Engl.* **1996**, *35*, 1947–1949.

[9] J. F. Guo, W. F. Yeung, S. Gao, G. H. Lee, S. M. Peng, M. H. W. Lam, T. C. Lau, *Eur. J. Inorg. Chem.* **2008**, 158–163.

[10] W. F. Yeung, H. K. Kwong, T. C. Lau, S. Gao, L. Szeto, W. T. Wong, *Polyhedron* **2006**, *25*, 1256–1262.

[11] N. Re, R. Crescenzi, C. Floriani, H. Miyasaka, N. Matsumoto, *Inorg. Chem.* **1998**, *37*, 2717–2722.

[12] M. Ferbinteanu, H. Miyasaka, W. Wernsdorfer, K. Nakata, K. Sugiura, M. Yamashita, C. Coulon, R. Clérac, *J. Am. Chem. Soc.* **2005**, *127*, 3090–3099.

[13] a) H.-Z. Kou, B. C. Zhou, S. Gao, D.-Z. Liao, R.-J. Wang, *Inorg. Chem.* **2003**, *42*, 5604–5611; b) B. Chiari, A. Cinti, O. Iovesana, P. F. Zanazzi, *Inorg. Chem.* **1995**, *34*, 2652–2657; c) A. Caneschi, D. Gatteschi, M. C. Melandri, P. Rey, R. Sessoli, *Inorg. Chem.* **1990**, *29*, 4228–4234.

[14] O. Kahn, *Molecular Magnetism*, VCH, Weinheim, **1993**.

[15] Z.-H. Ni, H.-Z. Kou, L. Zheng, Y.-H. Zhao, L.-F. Zhang, R.-J. Wang, A.-L. Cui, O. Sato, *Inorg. Chem.* **2005**, *44*, 4728–4736.

[16] W. W. Ni, Z. H. Ni, A. L. Cui, X. Liang, H. Z. Kou, *Inorg. Chem.* **2007**, *46*, 22–33.

[17] R. Sessoli, D. Gatteschi, *Angew. Chem.* **2003**, *115*, 278–309; *Angew. Chem. Int. Ed.* **2003**, *42*, 268–297.

[18] B. Wang, H. Wei, M. Wang, Z. Chen, *J. Chem. Phys.* **2005**, *122*, 204310–8.

[19] a) M. A. Watson, N. C. Handy, A. J. Cohen, *J. Chem. Phys.* **2003**, *119*, 6475–6481; b) A. J. Cohen, N. C. Handy, *Mol. Phys.* **2001**, *99*, 607–615.

[20] J. Lewis, F. E. Mabbs, A. Richard, *J. Chem. Soc. A* **1967**, 1014–1018.

[21] K. Srinivasan, P. Michaud, J. K. Kochi, *J. Am. Chem. Soc.* **1986**, *108*, 2309–2320.

[22] SHELX-97, G. M. Sheldrick, Göttingen University, Göttingen, **1997**.

[23] Amsterdam Density Functional (ADF), Version 2004.01, Scientific Computing and Modeling, Theoretical Chemistry, Vrije Universiteit, Amsterdam, **2007**.

[24] S. H. Vosko, L. Wilk, M. Nusair, *Can. J. Phys.* **1980**, *58*, 1200–1211.

[25] a) J. P. Perdew, J. A. Chevary, S. H. Vosko, K. A. Jackson, M. R. Pederson, D. J. Singh, C. Fiolhais, *Phys. Rev. B* **1992**, *46*, 6671–6687; b) C. Adamo, V. Barone, *J. Chem. Phys.* **1998**, *108*, 664–675.

Received: July 23, 2009
Published online: February 5, 2010

